Electronic supplementary information

Coordination Unsaturation of Vanadium Nitride Quantum Dots Boosts Low-Temperature Aerobic Oxidation of Thiophenic Sulfides

Huawei Yang,[a,b] Jiabao Bai,[a] Qinghua Zhang,[c] Lixia Yang,[a] Liangjiu Bai,[a] Donglei Wei,[a] Wenxiang Wang,[a] Ying Liang,[a] Lin Gu,[c] Hou Chen,*[a] and Shaojun Guo*[b]

[a] School of Chemistry and Materials Science, Ludong University, Yantai, 264025 P. R. China.

[b] School of Materials Science and Engineering, Peking University, Beijing, 100871 P. R. China.

[c] Institute of Physics, Chinese Academy of Sciences, Beijing, 100190 P. R. China.

Experimental Procedures

Synthesis of VN QDs/rGO and the counterparts

Briefly, 5 mL of GO nanosheets dispersion (10 mg/mL) was added into 45 mL pure water containing 3 mg of NH_4VO_3, and sonicated for 15 min. Then, the precursor dispersion was freeze-dried to form a sponge. Subsequently, VN QDs/rGO was obtained by annealing the precursor at 800 °C for 3 h under NH_3/Ar (4:6) atmosphere. VN NPs/rGO was prepared by the similar method to VN QDs/rGO by increasing the dosage of NH_4VO_3 to 15 mg. Neat rGO was prepared by the same approach for the preparation of VN QDs/rGO without adding NH_4VO_3. V_2O_5/rGO was prepared by a hydrothermal method. Briefly, 5 mL of GO nanosheets dispersion (10 mg/mL) was added into 45 mL pure water containing 5 mg of NH_4VO_3, and sonicated for 15 min. The pH value was adjusted to 2 with HCl aqueous solution (1 M). Then, the dispersion was transferred into a 45 mL autoclave and heated at 180 °C for 2 h. The products were washed with distilled water and ethanol three times.

Characterization of materials

The loading of V on the catalysts was quantitatively measured by an ICP-AES instrument (ICPE-9000, Shimadzu). All the solids were dissolved in a 3:1 mixture of HNO_3 and HCl under sonication until complete dissolution. The crystalline structure of the samples was observed by powder XRD patterns recorded on a Bruker D8 Advance diffractometer with Cu-Kα radiation (λ = 1.54060 Å). The data was collected within the 2θ range of 10-80° with an angular step size of 0.02°. XPS data were acquired on an EscaLab Xi+ instrument (Thermo fisher), using a monochromatic Al-Kα (1486.6 eV) radiation. TEM images were obtained using a Talos F200X G2 (Thermo Fisher Scientific) with an accelerating voltage of 200 kV, while HAADF-STEM images were recorded using a Titan cubed G2 60-300 (FEI) with an accelerating voltage of 300 kV. ESR spectra were recorded on an A300-10/12 spectrometer (Bruker). The catalysts were dispersed in the reaction system with the content of 5 mg/mL, and then 0.5 mL of the dispersion was added to a nuclear magnetic tube. The corresponding gas was introduced at the rate of 2 mL/min. The ESR spin trapping tests were operated at X-band frequency and magnetic field modulation of 9.856 GHz, with a microwave power of 19.36 mW and modulation amplitude of 1 G. The continuous-wave ESR tests were performed by rapidly cooling the above reaction system by liquid helium, and operated at X-band frequency and magnetic field modulation of 9.853 GHz, with a microwave power of 23.16 mW and modulation amplitude of 1 G. The resonance lines were simulated by the Easyspin software. XAFS spectra data (V K-edge) were collected at the BL14W1 station in Shanghai Synchrotron Radiation Facility (SSRF, operated at 3.5G eV with a maximum current of 300 mA). The data were collected at room temperature (25 °C) in transmission mode using a N_2-filled ionization chamber).

Catalyst testing

Aerobic oxidation of sulfides was studied at atmospheric pressure in a 50 mL three-neck flask equipped with a gas injection, a reflux tube and a sampling port for liquid. The sulfides were dissolved in decahydronaphthalene to reach 500±5 ppm of sulfur content. In a general test, 30 mL of model oil and 2 mg of catalyst were charged into the flask and sonicated for 15 min. The flask was then immersed in an oil bath to control the desired reaction temperature (60-110 °C) and magnetically stirred at 500 rpm, while high purity N_2 was bubbled into the flask before the temperature of the reaction system reached the set value. To start the reaction, N_2 was replaced by air, which was pretreated by a silica gel column and a 4 A molecular sieve column in series to remove moisture. The flow rate of air was controlled at 40 mL/min with a precision flow meter. Samples were taken from the liquid phase at 30 minute intervals, and GC-FID (Agilent 7890A; column: HP-5, FID: Agilent) was used to quantify the conversion of sulfides without considering the selectivity to sulfones or sulfoxides. Each experiment was repeated at least three times. GC-MS (Agilent 7890A; HP-5ms, MS: Agilent 5975C) was used to identify the products in the reaction. The conversion rate of the sulfides was calculated as follows:

$$S_{conv} = \frac{C_0 - C_t}{C_0} \times 100\%$$

where S_{conv} is the conversion of sulfides (%), C_0 and C_t were mass concentrations of sulfides before and after reaction began for certain time (mg/L), respectively.

Desulfurization of real diesel

The reaction procedure for real diesel was similar to that for model fuel. The catalyst dosage was 20 mg instead of 2 mg in order to achieve rapid conversion of sulfides. The reaction temperature was set as 80 °C, since a reaction at 80 °C can be facilely realized in the petroleum industry by using waste heat without consuming extra energy. The total sulfur content was quantitatively analyzed by using multi EA 5000 elemental analyzer (Analytical Jena). The concentration and evolution of sulfur species were determined by a GC-7820 instrument (Huifen; column: HP-5; detector: FPD).

Reuse of catalysts

After each recycle run, the reaction system was transferred into a centrifugal tube, and the catalyst was separated by centrifugation. Then, fresh diesel was added into the centrifugal tube to redisperse the catalyst, and the dispersion was transferred into the reaction flask to start a new cycle. The reaction flask and centrifuge tube were not washed during the entire recycle experiment to minimize catalyst loss.

XAFS measurement and data analysis

XAFS spectra data (V K-edge) were collected at the BL14W1 station in Shanghai Synchrotron Radiation Facility (SSRF, operated at 3.5GeV with a maximum current of 300 mA). The data were

collected at room temperature (25 °C) in transmission mode using a N_2-filled ionization chamber). All samples were pelletized as disks of 13 mm diameter and 1 mm thickness using graphite powder as a binder.

The acquired EXAFS data were processed according to standard procedures using the ATHENA module implemented in the IFEFFIT software package. The EXAFS spectra were obtained by subtracting the post-edge background from the overall absorption and then normalizing with respect to the edge-jump step. Subsequently, the $\chi(k)$ data were Fourier-transformed to real (R) space using a Hanning window (dk = 1.0 Å^{-1}) to separate the EXAFS contributions from different coordination shells. To obtain the quantitative structural parameters around the central atoms, least-squares curve parameter fitting was performed using the ARTEMIS module of the IFEFFIT software package. The following EXAFS equation was used:

$$\chi(k) = \sum_j \frac{N_j S_0^2 F_j(k)}{kR_j^2} \exp[-2k^2\sigma_j^2] \exp[\frac{-2R_j}{\lambda(k)}] \sin[2kR_j + \varphi_j(k)]$$

where S_0^2 is the amplitude reduction factor; F_j(k) is the effective curved-wave backscattering amplitude, N_j is the number of neighbours in the j^{th} atomic shell, R_j is the distance between the X-ray absorbing central atom and the atoms in the j^{th} atomic shell (backscatterer), λ is the mean free path (in Å), ϕ_j(k) is the phase shift (including the phase shift for each shell and the total central atom phase shift) and σ_j is the Debye–Waller parameter of the j^{th} atomic shell (variation of distances around the average R_j). The functions F_j(k), λ and ϕ_j(k) were calculated with the ab initio code FEFF8.2.

DFT calculation

Spin polarized DFT calculations were conducted using the projector augmented-wave method (PAW) as implemented in the Vienna Ab initio Simulation Package (VASP) code, while the functional of choice was Perdew–Becke–Ernzerhof (PBE) with dispersion contributions introduced through the D3 approach.[1-5] The monoelectronic valence states were expanded as plane waves with a maximum kinetic energy of 520 eV. The slabs of VN on graphene were modelled using a 4 × 3× 1 supercell with 36 V atoms, 36 N atoms and 36 C atoms, and the slabs were separated by 20 Å of vacuum. The k-points sampling was a 2 × 3 × 1 grid. A dipole correction was employed along the z-direction normal to the slab faces. The optimization thresholds were 10^{-5} and 10^{-4} eV for electronic and ionic relaxations, respectively. The model of VN QD on graphene was modelled using with a hexagonal VN with 4 atom-layer thickness, which contained 36 V atoms, 36 N atoms and 160 C atoms. All the models were optimized to thresholds before the computation of adsorption process.

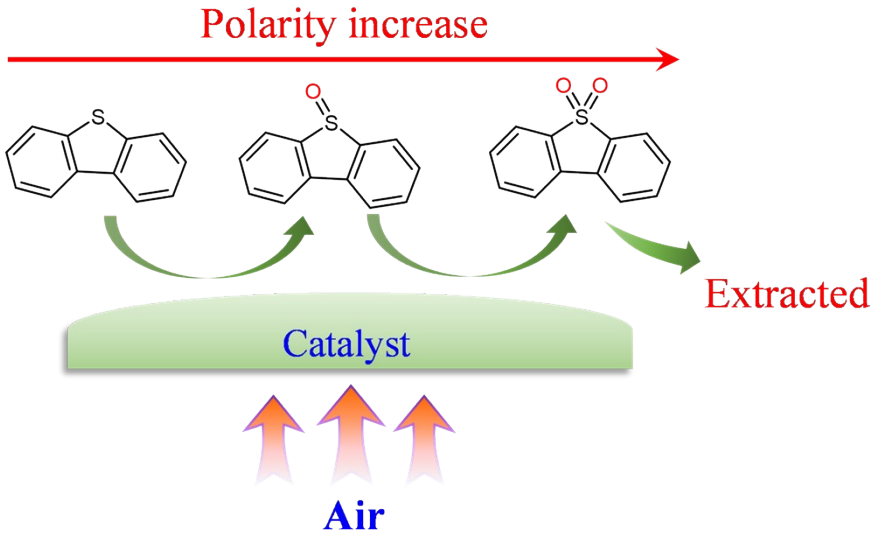

Fig. S1 Desulfurization principle of AODS.

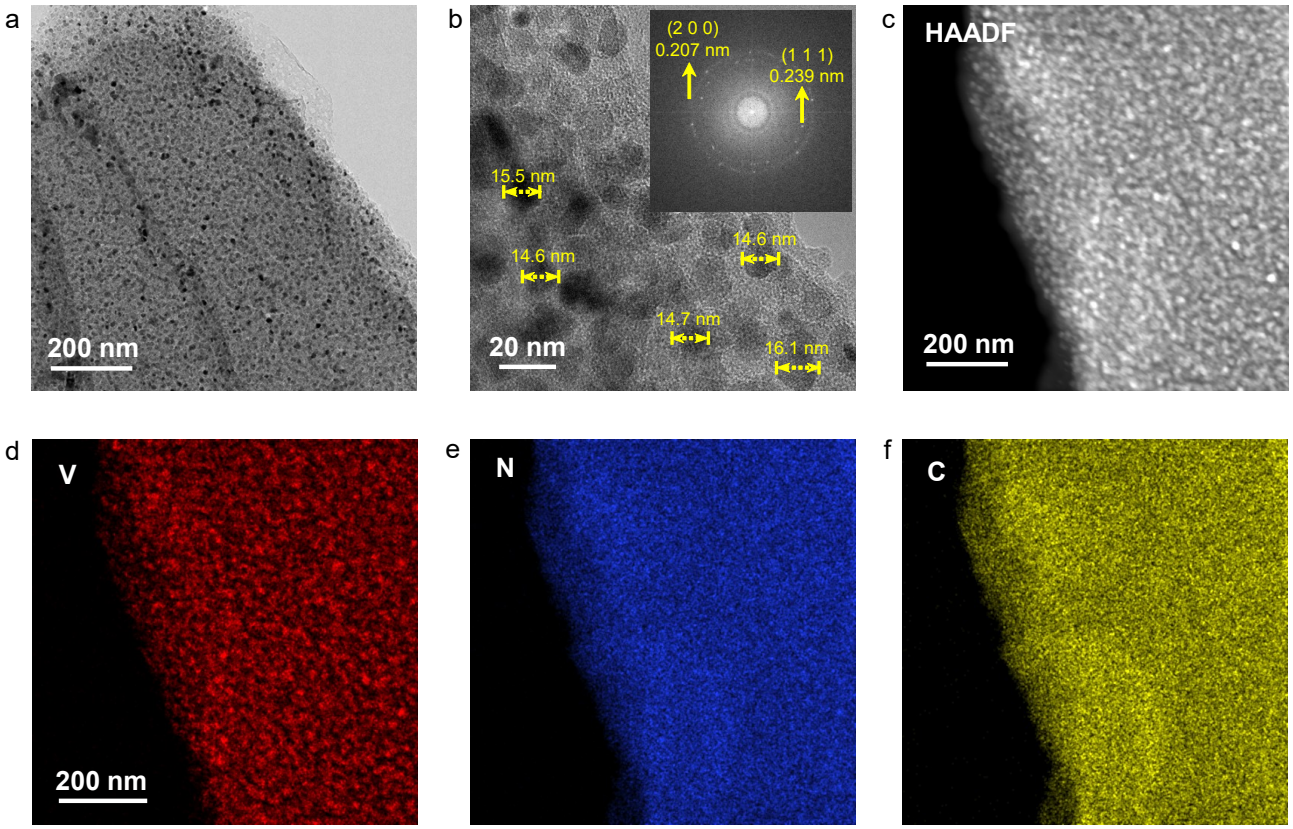

Fig. S2 Structural feature of VN NPs/rGO. (a) TEM, (b) HRTEM and (c) HAADF images. (d-f) EDS mapping images of V, N and C. Determined by the TEM images, the particle size of VN NPs on graphene is about 15 nm, larger than that of VN QDs (2 – 3 nm).

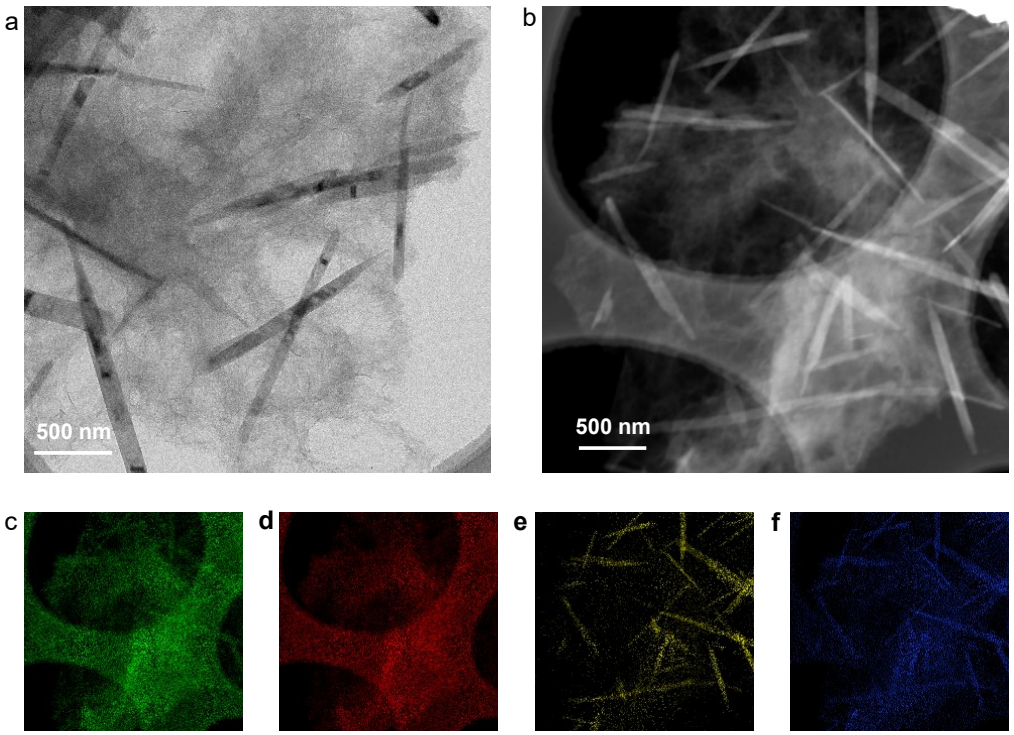

Fig. S3 Structural feature of V_2O_5/rGO. (a) TEM and (b) HAADF images. (c-f) EDS mapping images of N, C, V and O.

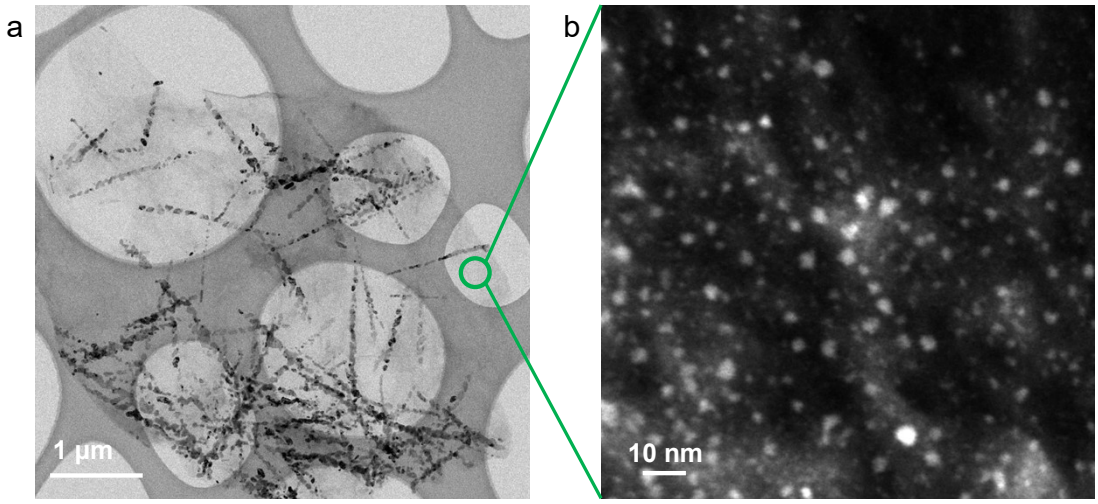

Fig. S4 Structural feature of the ammoniated V_2O_5/rGO. (a) TEM and (b) HAADF images. *Via* high temperature ammonization, the V_2O_5 nanowires were transformed into VN particles, while VN QDs were also observed on the graphene sheet. The result indicates that VN QDs were formed spontaneously at high temperatures.

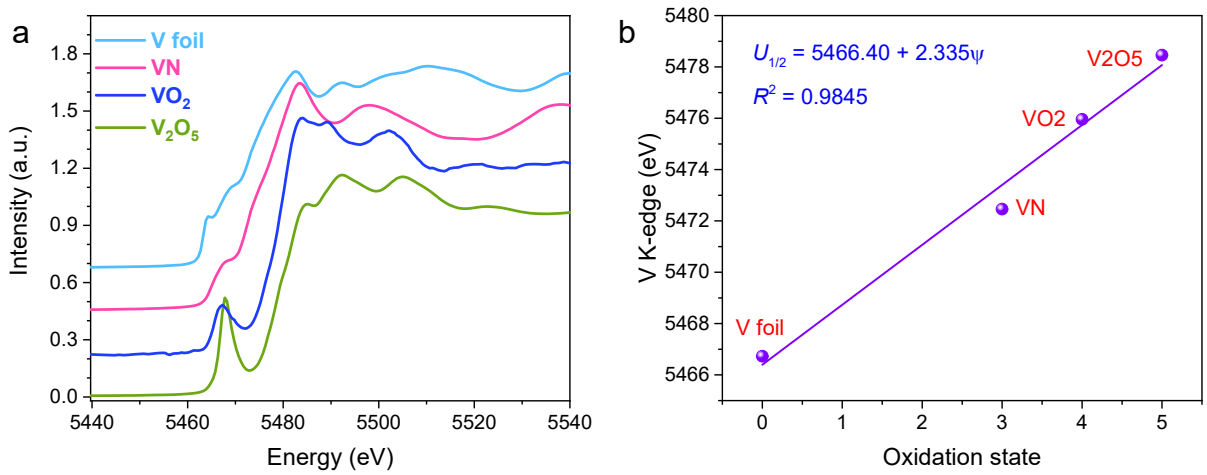

Fig. S5 Determining the oxidation state of V by XANES. (a) K-edge XANES spectra of the references including V foil, VN, VO_2 and V_2O_5. The determination of adsorption edge in the XANES spectra was based on the zero position of the second derivative of the near-edge spectra. (b) Correlation between the V oxidation state and the position of adsorption edge.

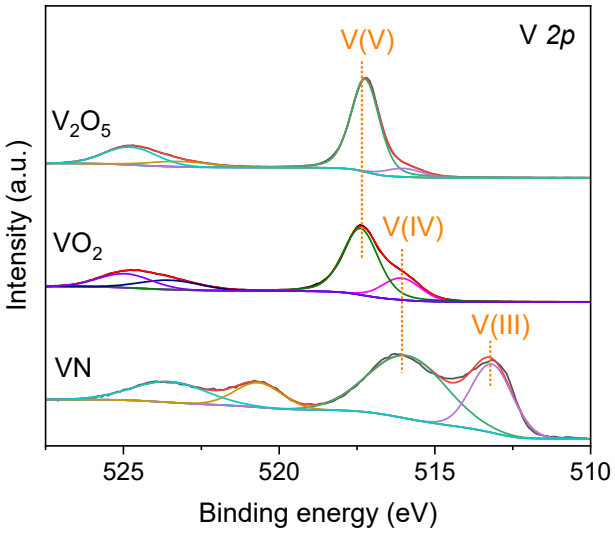

Fig. S6 Oxidation state of V determined by XPS. The V 2p peak positions of V(III), V(IV) and V(V) are extracted from the XPS spectra of VN, VO_2 and V_2O_5, respectively.

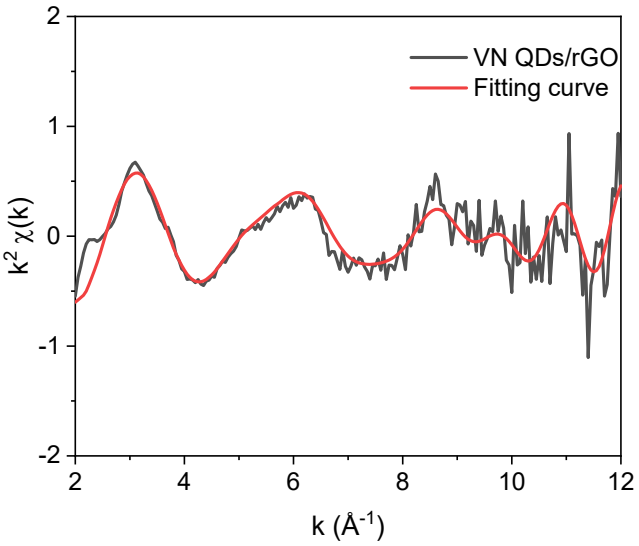

Fig. S7 K space fitting curve of VN QDs/rGO.

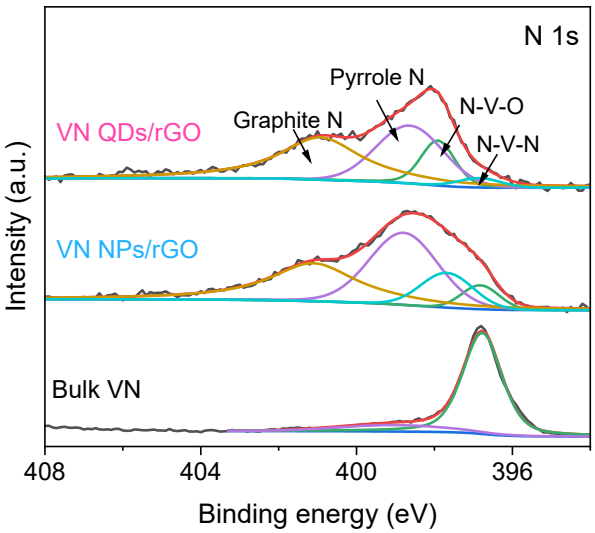

Fig. S8 N1s XPS curves of the indicated samples. The graphitic N and pyrrole N are assigned to the N atoms doped in graphene. The N-V-N group corresponds to the lattice N inside the VN crystal, consistent with the N 1s curve of bulk VN. The O-V-N group is existed at the surface of VN, which originated from the exchange of lattice N into O.

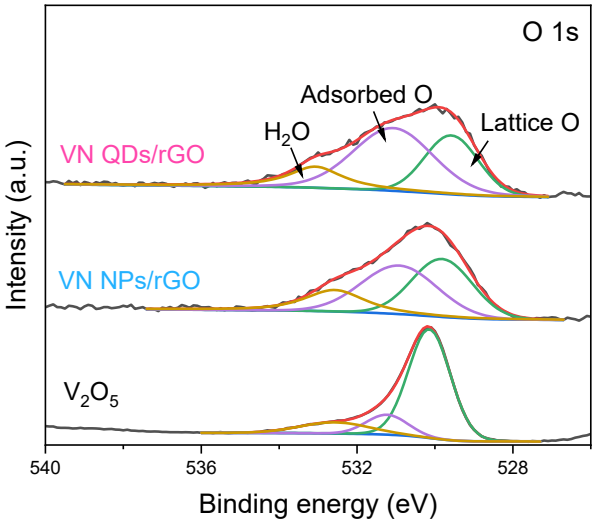

Fig. S9 O1s XPS curves of the indicated samples. The O 1s curves are deconvoluted to three peaks at around 529.6, 530.9 and 532.7 eV, respectively, corresponding to the lattice O, adsorbed oxygen and adsorbed water. For an aerobic catalyst, the proportion of adsorbed oxygen species reflects the capability to absorb and bind O_2, and therefore has a significant correlation with the activity in the oxygen-demanding reactions. The proportion of adsorbed oxygen in VN QDs/rGO is much higher than that of VN NPs/rGO and V_2O_5, indicating a higher surface polarity, and boosting the O_2 activation.

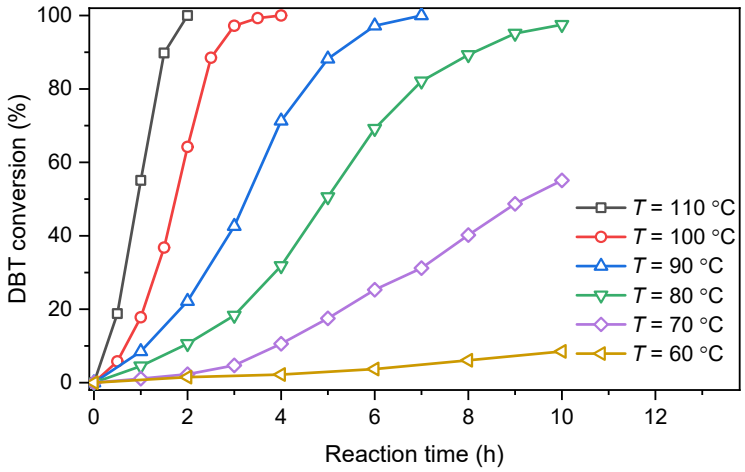

Fig. S10 Catalytic performance of VN QDs/rGO at different temperatures upon the aerobic oxidation of DBT. Reaction conditions: m_{catal} = 2 mg, V_{oil} = 30 mL, initial S-content = 500 ppm, F_{air} = 40 mL/min. VN QDs/rGO still has a considerable catalytic performance at 70 °C, while the catalytic efficiency was attenuate at 60 °C, reaching a DBT conversion of 8.6% in 10 hours. Therefore, the minimum conversion temperature was identified as 70 °C.

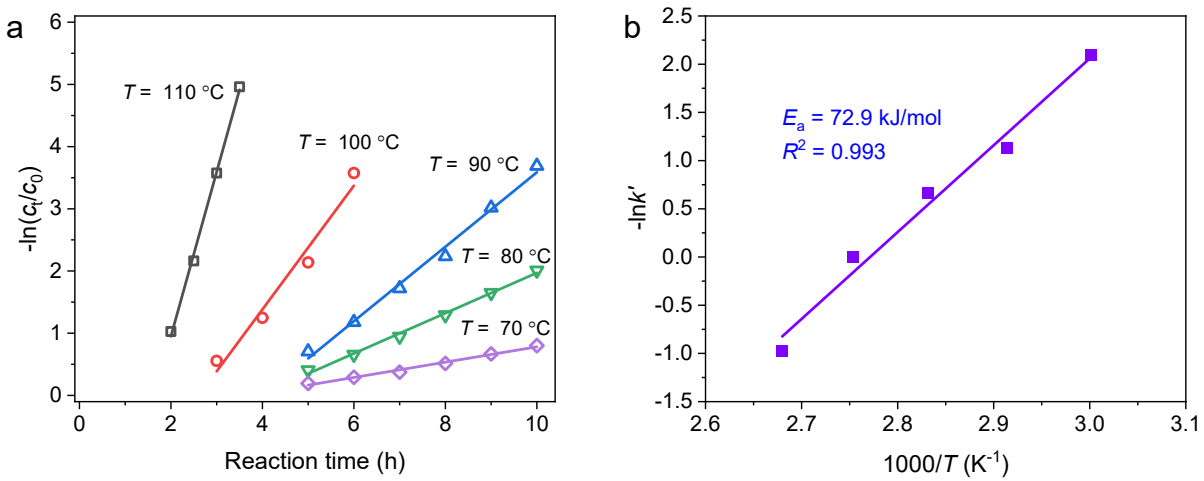

Fig. S11 Kinetics analysis of DBT aerobic oxidation over the catalyst. (a) Fitting of reaction constants with the first-order kinetics equation. (b) Fitting of apparent activation energy with the Arrhenius equation.

Reaction kinetics method was applied to assist with the reaction evaluation of the catalyst for its catalytic capacity in the ODS system. In general, the ODS reaction was identified with first order kinetics according to previous researches. The reaction rate of DBT oxidation with air as an oxidant is expressed as

$$-\frac{dc_{DBT}}{dt} = kc_{DBT}c_{oxy}$$

where, C_{oxy} and C_{DBT} represented the concentrations of oxygen and DBT in the reaction system, while k refers to the reaction rate constant (h^{-1}).

For the excess O_2 at constant flow rate, the equation was simplified as

$$-\frac{dc_{DBT}}{dt} = k'c_{DBT}$$

where k' indicates the apparent rate constant (h^{-1}).

Then, the activation the reaction was fitted, and the reaction rate constants at different temperatures were calculated. The apparent activation energy was calculated to be 72.9 kJ/mol.

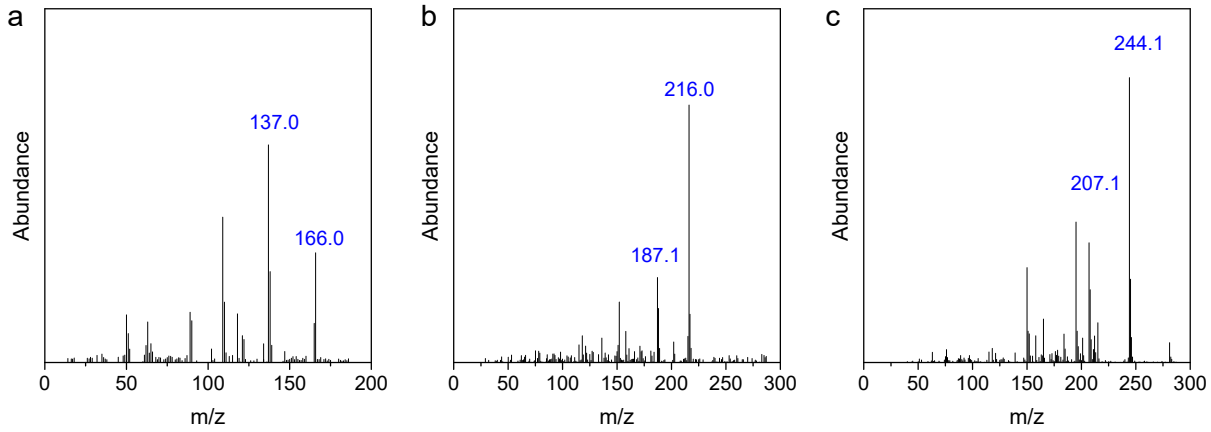

Fig. S12 Identification of oxidation products of different sulfides by GC-MS. (a – c) Mass spectra of the oxidation products of BT, DBT and 4,6-DMDBT, respectively.

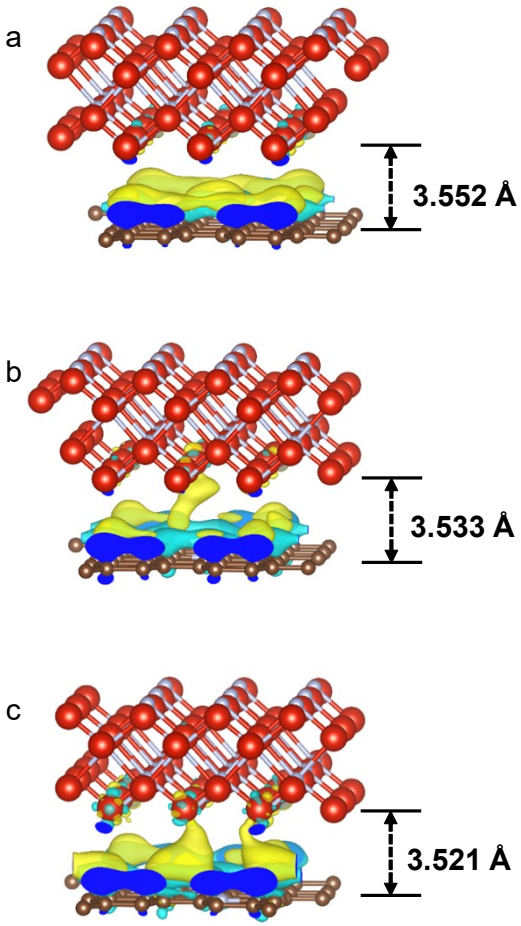

Fig. S13 The optimized coordinate structures of VN supported on graphene with different numbers of N atom. (a) VN/G, (b) VN/N1G and (c) VN/N2G, whose N atom numbers are 0, 1 and 2, respectively.

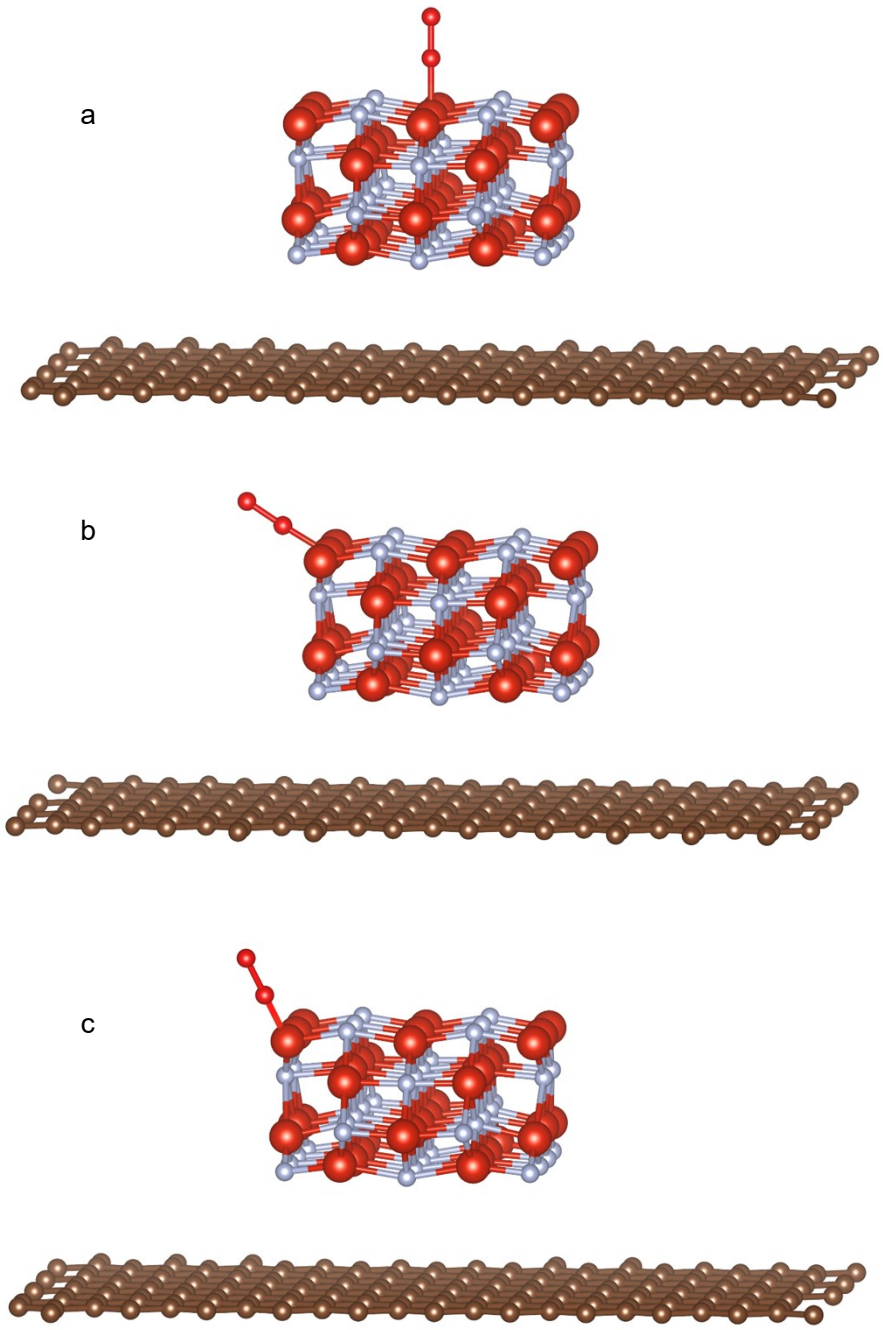

Fig. S14 The optimized coordinate structures of O_2 adsorbed on VN QDs/rGO. O_2 adsorbed on (a) surface site, (b) edge site and (c) corner site.

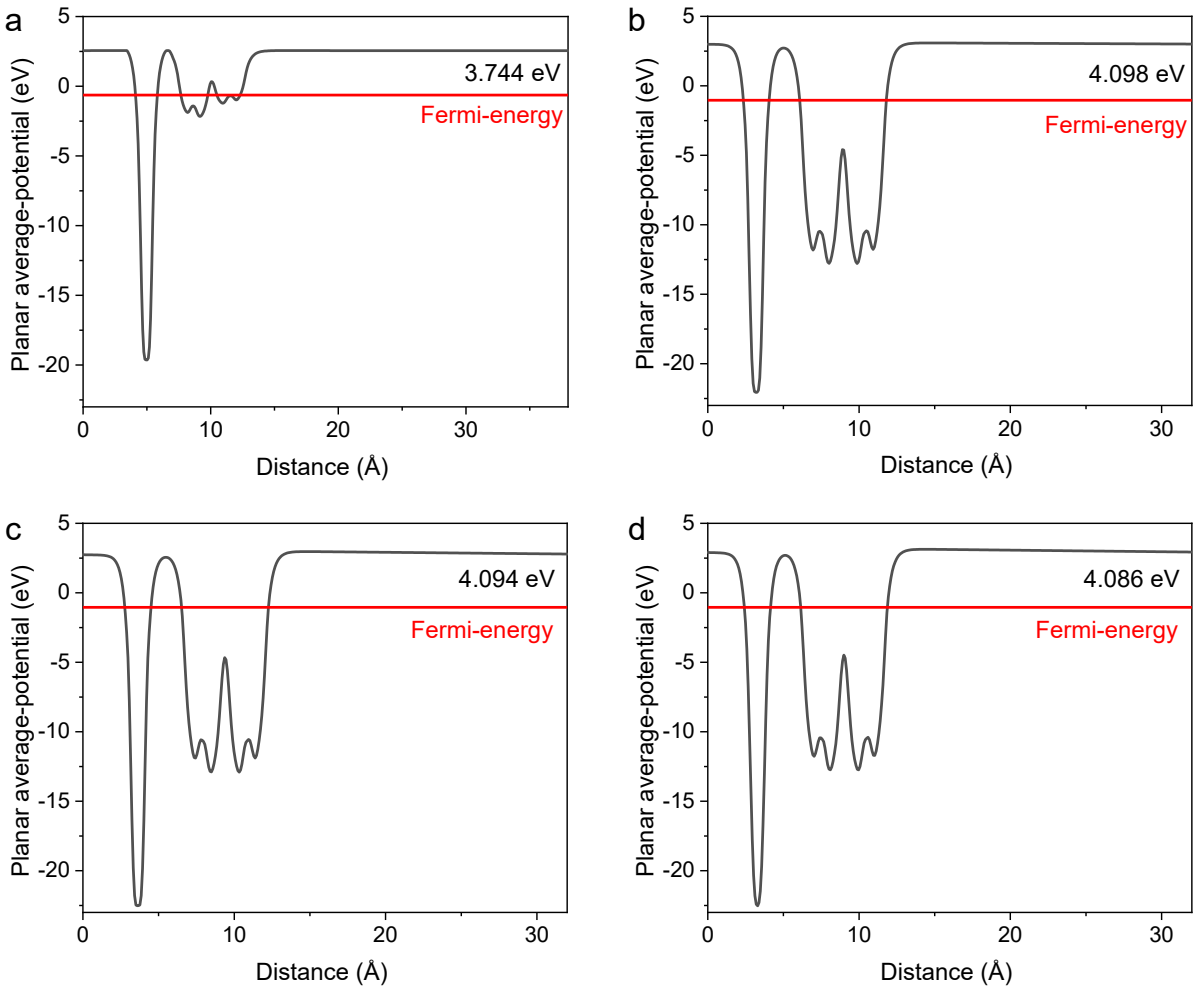

Fig. S15 Determination of *WF*s with planar average-potential diagrams. (a) VN QD/rGO, (b) VN/G, (c) VN/N1G and (d) VN/N2G.

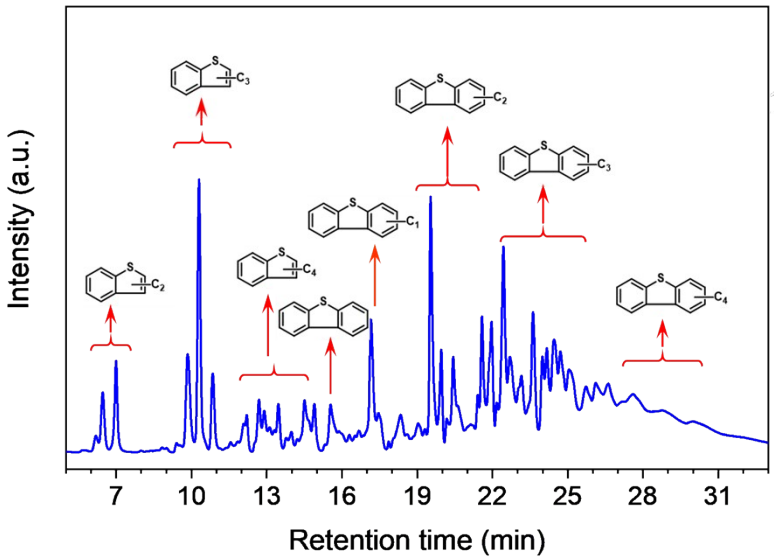

Fig. S16 Distribution of sulfides in the original diesel.

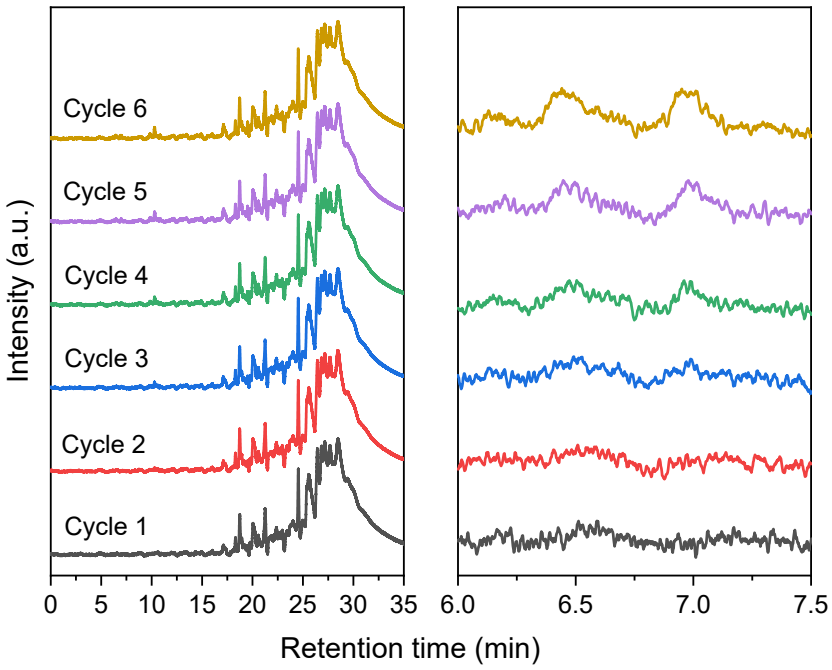

Fig. S17 Reuse of VN QDs/rGO in AODS of the diesel. Left: GC-FPD chromatograms of the oxidized diesel after each repeated cycle; right: local enlarged GC-FPD chromatograms.

Table S1 Loading amount of V in the samples determined by ICP-OES.

Sample	V content (wt.%)
VN QDs/rGO	2.85 ± 0.09
VN NPs/rGO	15.17 ± 0.24
V_2O_5/rGO	5.63 ± 0.17

Table S2 Oxidation state of V in the indicated samples determined by XANES and XPS.

Sample	XANES	XPS		
	Average oxidation state	V(III)	V(IV)	V(V)
VN QDs/rGO	3.85	28.3%	71.7%	-
VN NPs/rGO	3.48	48.5%	51.5%	-
V_2O_5/rGO	-	-	9.7%	90.3%
Bulk VN	-	59.3%	40.7%	-

Table S3 Comparison of catalytic performances of VN QDs/rGO with the previous V-based catalysts.

Catalyst	Oxidant	Reaction parameters and DBT Conversion	Mass specific activity /mmol g^{-1} h^{-1}	*TOF* /h^{-1}	Ref
VN QDS/rGO	Air	70 °C, 2 mg/30 mL, 10 h, 82.2%	19.22	40.84	This work
VN QDS/rGO	Air	80 °C, 2 mg/30 mL, 9 h, 82.2%	26.04	55.34	This work
VN QDS/rGO	Air	90 °C, 2 mg/30 mL, 7 h, 82.2%	33.48	83.01	This work
VN QDS/rGO	Air	100 °C, 2 mg/30 mL, 4 h, 82.2%	58.59	124.51	This work
VN QDS/rGO	Air	110 °C, 2 mg/30 mL, 2.5 h, 82.2%	93.74	199.22	This work
V_2O_5/BNNS	Air	110 °C, 200 mg/50 mL, 4 h, 70.6%	0.97	0.70	[6]
V8@iPAF	O_2	80 °C, 2 mg/6 mL, 5 h, 100%	9.38	1.91	[7]
Atomic-layered V_2O_5	Air	120 °C, 10 mg/50 mL, 4 h, 99.7%	19.53	1.99	[8]
Pt- V_2O_5	Air	110 °C, 0.6 mg/1 mL, 5 h, 99.2%	5.21	0.53	[9]
V_2O_5 BM-3	Air	120 °C, 30 mg/50 mL, 4 h, 99.7%	6.51	0.66	[10]
$[C_8H_{17}N(CH_3)_3]_3H_3V_{10}O_{28}$	O_2	80 °C, 40 mg/20 mL, 1.3 h, 100%	2.61	0.27	[11]
$[C_8mim]_3H_3V_{10}O_{28}$/g-BN	Air	120 °C, 80 mg/40 mL, 4 h, 100%	1.95	3.05	[12]
$[C_8H_{17}N(CH_3)_3]_3HIV_9O_{28}$	O_2	80 °C, 40 mg/20 mL, 2.5 h, 100%	3.13	0.55	[13]
$Q_5H_4PV_{14}O_{42}$	O_2	80 °C, 40 mg/20 mL, 3 h, 100%	2.60	0.44	[14]
MFM-300(V)	O_2	120 °C, 0.75g/L, 5 h, 100%	4.17	0.97	[15]

The reaction parameters include reaction temperature, catalytic dosage/model oil usage and reaction time.

Mass specific activity (mmol g^{-1} h^{-1}) and turnover frequency (*TOF*, h^{-1}) are calculated as follows:

$$\text{Mass specific activity(mmol g}^{-1}\text{ h}^{-1}) = \frac{S_{\text{conv}} \times C_0 \times V_{\text{oil}} / t}{m}$$

$$TOF(\text{h}^{-1}) = \frac{S_{\text{conv}} \times C_0 \times V_{\text{oil}} / t}{m \times \omega / M_{\text{V}}}$$

S_{conv}: conversion of sulfides;

C_0: initial sulfur content, mol L^{-1};

V_{oil}: volume of model oil addition, L;

t: reaction time, h;

m: mass of catalyst dosage, g;

ω: V loading in the catalyst;

M_V: atomic mass of V, 50.94 g mol^{-1}.

Table S4 Adsorption energy, bond length and charge transfer of O_2 and DBT adsorbed on different sites.

Site	$E_{o,ad}$ (eV)	O-O bond length	Charge difference O1	Charge difference O2	$E_{DBT,ad}$ (eV)
A1	0.43	1.269	0.325	0.151	0.48
A2	0.67	1.285	0.339	0.189	0.46
A3	0.71	1.289	0.350	0.200	0.41
S1	1.32	1.311	0.411	0.298	0.65
S2	1.59	1.325	0.469	0.352	1.67
S3	1.88	1.344	0.502	0.403	1.93

Table S5 Sulfur species in the original diesel determined by GC-FPD.

Sulfur species	S-content distribution (wt. %)
BT	0.860
C1BT	1.950
C2BT	9.610
C3BT	19.201
C4BT	8.176
DBT	4.637
C1DBT	12.348
C2DBT	18.899
C3DBT	13.477
C4DBT	7.064
≥ C5DBT	3.782

Table S6 Sulfur-content of diesels analyzed by an elemental analyzer.

Sample	Sulfur content /ppm	
	Original diesel	Oxidized diesel
Before extraction	577.6 ± 3.4	545.9 ± 3.1
After extraction	98.8 ± 1.9	7.7 ± 0.9

The extraction of diesel was performed using methanol with a volume ratio of 1:2 (diesel / methanol). The sulfur content of the oxidized hydrogenation diesel was reduced to 7.7 ppm after extraction, which meets the most stringent standards for transportation fuels (≤ 10 ppm).

References

1. P. E. Blochl, *Phys. Rev. B*, 1994, **50**, 17953-17979.
2. G. Kresse and J. Furthmuller, *Phys. Rev. B*, 1996, **54**, 11169-11186.
3. G. Kresse and J. Furthmüller, *Comp. Mater. Sci.*, 1996, **6**, 15-50.
4. J. P. Perdew, K. Burke and M. Ernzerhof, *Phys. Rev. Lett.*, 1996, **77**, 3865-3868.
5. S. Grimme, *J. Comput. Chem.*, 2006, **27**, 1787-1799.
6. C. Wang, Y. Qiu, H. Wu, W. Yang, Q. Zhu, Z. Chen, S. Xun, W. Zhu and H. Li, *Fuel*, 2020, **270**, 117498.
7. J. Song, Y. Li, P. Cao, X. Jing, M. Faheem, Y. Matsuo, Y. Zhu, Y. Tian, X. Wang and G. Zhu, *Adv. Mater.*, 2019, **31**, 1902444.
8. C. Wang, H. P. Li, X. J. Zhang, Y. Qiu, Q. Zhu, S. H. Xun, W. S. Yang, H. M. Li, Z. G. Chen and W. S. Zhu, *Energy Fuels*, 2020, **34**, 2612-2616.
9. C. Wang, W. Jiang, H. X. Chen, L. H. Zhu, J. Luo, W. S. Yang, G. Y. Chen, Z. G. Chen, W. S. Zhu and H. M. Li, *Chinese J. Catal.*, 2021, **42**, 557-562.
10. Y. Zou, C. Wang, H. Chen, H. Ji, Q. Zhu, W. Yang, L. Chen, Z. Chen and W. Zhu, *Green Energy Environ.*, 2021, **6**, 169-175.
11. N. F. Tang, Y. N. Zhang, F. Lin, H. Y. Lu, Z. X. Jiang and C. Li, *Chem. Commun.*, 2012, **48**, 11647-11649.
12. C. Wang, Z. G. Chen, X. Y. Yao, Y. H. Chao, S. H. Xun, J. Xiong, L. Fan, W. S. Zhu and H. M. Li, *Fuel*, 2018, **230**, 104-112.
13. N. F. Tang, Z. X. Jiang and C. Li, *Green Chem.*, 2015, **17**, 817-820.
14. N. F. Tang, X. P. Zhao, Z. X. Jiang and C. Li, *Chinese J. Catal.*, 2014, **35**, 1433-1437.
15. X. L. Li, Y. L. Gu, H. Q. Chu, G. Ye, W. Zhou, W. Xu and Y. Y. Sun, *Appl. Catal. A-Gen.*, 2019, **584**, 117152.